

# Study on Rupture of Tube Type Crash Energy Absorber using Finite Element Method

Won Mok. Choi, Tae Su. Kwon, Hyun Sung. Jung, and Jin Sung. Kim

**Abstract**—The aim of this paper is to confirm the effect of key design parameters, the punch radius and punch angle, on rupture of the expansion tube using a finite element analysis with a ductile damage model. The results of the finite element analysis indicated that the expansion ratio of the tube was mainly affected by the radius of the punch. However, the rupture was more affected by the punch angle than the radius of the punch. The existence of a specific punch angle, at which rupture did not occur, even if the radius of the punch was increased, was found.

**Keywords**— Expansion tube, Ductile damage, Shear failure, Stress triaxiality.

## I. INTRODUCTION

TUBE expansion is a plastic working process in which two tubes with different sizes are joined together or a tube's end is molded for special purposes. Expansion tubes are widely used as crash energy absorption members in the automobile and railway industries on the bases of their uniform force and high specific energy generated during expansion. Expansion tubes absorb crash energy with the plastic strain energy and the friction energy generated when a punch with larger outer diameter than the tube's inner diameter expands the tube. The plastic strain energy is proportional to the expansion ratio, which is defined as  $R_p/R_a$  ( $R_a$ : tube outer diameter before expansion,  $R_p$ : tube outer diameter after expansion), while the expansion ratio varies depending on the punch's outer diameter, tube thickness, and the tube's inner diameter. Upon energy absorption by the expansion tube, if the expansion ratio is too great, or the punch's direction does not match the tube's axial direction, the tube will rupture at the early stage or in the mid-period of expansion. Such a rupture occurs because the plastic strain is larger than the failure strain, and the tube's rupture is greatly influenced by mechanical characteristics of the material as well as the expansion ratio.

M Shakeri and S Salehghaffari et al. confirmed the effects of three contact conditions – blasting, no surface treatment, and coating – on the expansion tube's energy absorption through quasi-static tests, and suggested a numerical model [1]. In

addition, Vojkan Lucanin and Jovan Tanaskovic et al. performed studies on an expansion tube's energy absorption characteristics through quasi-static tests and crash tests [2]. A. Karrech and A. Seibi devised a numerical model that can predict the tube's indentation load and absorbed energy, and suggested the punch's optimal shape [3]. T. Daxner and F.G. Rammerstorger et al. studied how a tube's length affects local buckling and necking instability, which occur at the tube upon the end process, through quasi-static tests and the finite element method [4]. B.P.P. Alemeida and M.L. Alves et al. performed quasi-static tests and a finite element analysis to confirm how a punch affects buckling and rupture, which are end forming limits [5].

Prior research mainly dealt with the effects of the contact conditions between a tube and a punch, or the effect that the strain rate has on energy absorption characteristics and on the tube's ultimate forming limits. In the process of energy absorption by the expansion tube, the punch shape has a great effect not only on the energy absorption but also on the tube's rupture. Therefore, in order to absorb crash energy in a stable manner, studies on how a punch's shape influences a tube's strain must be carried out.

ABAQUS/explicit, a commercial finite element program, was used in this study to examine the effects of the punch radius and angle, the main design factors determining a punch's shape, on the strain and rupture of the expansion tube in an analytical manner. They also determined whether rupture of the tube will occur by applying a damage initiation criterion, a damage model for materials to predict rupture of ductile materials, and the shear failure model [6, 7]. To confirm the effect of the punch radius, a finite element analysis was performed by varying the radius as 105mm, 107.5mm, 110mm, and 115mm, and another finite element analysis was performed for punch angles of 15°, 30°, 45° and 50°. In addition, to precisely predict the damage and rupture of materials, a tensile test was performed on three specimens with different stress triaxiality to determine main factors for the damage model required for the finite element analysis.

## II. MATERIAL AND DAMAGE MODEL

### A. Material

As the first step to create an expansion tube, forge processed SCM440 materials were deep-hole processed and then heat-treated to enhance the tube's ductility. Lastly, a precision mechanical process was carried out to complete the manufacture of the expansion tube. In order to examine

W. M. Choi is with University of Science and Technology, 113 Gwahak-ro, Yuseong-gu, Daejeon, Korea (phone: +82-31-460-5274; fax: +82-31-460-5289; e-mail: wmchoi@krii.re.kr).

T. S. Kwon is with Korea Railroad Research Institute, 360-1 Woram-dong, Uiwang, Gyeonggi, Korea (e-mail: tskwon@krii.re.kr).

H. S. Jung is with Korea Railroad Research Institute, 360-1 Woram-dong, Uiwang, Gyeonggi, Korea (e-mail: jhs@krii.re.kr).

J. S. Kim is with Korea Railroad Research Institute, 360-1 Woram-dong, Uiwang, Gyeonggi, Korea (e-mail: kjs@krii.re.kr).

mechanical characteristics of the heat-treated expansion tube, a dog-bone type tensile specimen was created and a standard tensile test was performed using a Universal Test Machine to calculate the true stress and true strain. The relations between true stress and true strain of the heat-treated SCM440 obtained from the tensile test were represented with the Holloman equation, in which  $K$  is 1GPa and  $n$  is 0.189 [8].

$$\bar{\sigma} = K \bar{\varepsilon}^n \quad (1)$$

**B. Damage model**

All tables and figures you insert in your document are only to help you gauge the size of your paper, for the convenience of the referees, and to make it easy for you to distribute preprints.

A microscopic damage model is required to predict rupture of a ductile material such as SCM440. If the strain of the material reaches its ductile limit due to external factors, void nucleation occurs inside, followed by void growth caused by plastic deformation. If the void continues to grow and void coalescence occurs with neighboring voids, the material will ultimately rupture and will lose its load transfer capacity. In order to predict microscopic damage and rupture of ductile material using finite element analysis, methods suggested by Gurson-Tvergaard-Needleman [9-11], Rice and Tracey [12], and Cockroft and Latham [13], and shear failure model are often used. In an explicit finite element method, such a model of rupture calculates the failure parameter at the integral point of an element at each time increment, and once this parameter reaches a certain value, that element is eliminated from the model.

The study predicts damage and rupture of the expansion tube by using a damage initiation criterion and shear failure model. The shear failure model assumes that the material will rupture if the sum of equivalent strain calculated at the integral point reaches the failure strain. Eq. (2) shows the damage initiation criterion, which represents softening of the material as a result of damage.  $\bar{\varepsilon}_D^{pl}$  denotes the equivalent plastic strain where the damage starts, while  $\dot{\bar{\varepsilon}}^{pl}$  represents the strain rate. Meanwhile,  $\eta$  denotes the stress triaxiality defined by Eq. (3), while  $\sigma_H$  and  $\bar{\sigma}$  represent hydrostatic stress ( $\sigma_H = (\sigma_1 + \sigma_2 + \sigma_3)/3$ ) and equivalent stress

$$(\bar{\sigma} = \sqrt{1/2[(\sigma_1 - \sigma_2)^2 + (\sigma_2 - \sigma_3)^2 + (\sigma_3 - \sigma_1)^2]}), \text{ respectively.}$$

Eq. (4) shows the shear failure model, with  $\bar{\varepsilon}_f^{pl}$  representing the equivalent plastic strain where the rupture initiates [7]. Because the plastic strain of Eq. (2) and the failure strain of Eq. (4) are affected by the stress triaxiality, the change in the strain caused by the stress triaxiality needs to be applied to the finite element analysis in order to make a more precise prediction of the expansion tube [14, 15].

$$\omega_D = \int \frac{d\bar{\varepsilon}^{pl}}{\bar{\varepsilon}_D^{pl}(\eta, \dot{\bar{\varepsilon}}^{pl})} = 1 \quad (2)$$

$$\eta = \frac{\sigma_H}{\bar{\sigma}} \quad (3)$$

$$\omega = \frac{\bar{\varepsilon}_0^{pl} + \sum \Delta \bar{\varepsilon}^{pl}}{\bar{\varepsilon}_f^{pl}} = 1 \quad (4)$$

**III. CALIBRATION OF DAMAGE PARAMETERS**

**A. Specimen tests**

Fig. 1 shows that the failure strain varies depending on the stress's status (compressive, shear, and tensile) caused by change in the failure strain based on the stress triaxiality of ductile material. The stress triaxiality of the expansion tube verified by the finite element analysis changes from -0.3 to 0.67, but the range of the stress triaxiality of the tube's outer surface where the rupture takes place is divided into a range of high stress triaxiality between 0.33 ~ 0.67, as shown in Fig. 1. To obtain the failure strain of high stress triaxiality, tensile strength tests were performed on three specimens with notches ( $R=2, 4, \infty$ mm) and a finite element analysis was also carried out with the same conditions to calculate the stress triaxiality and failure strain. Fig. 2 shows the shapes of specimens used for the tensile test and Primary dimensions, and a UTM (Universal Test Machine) by INSTRON was used for the test and an extensometer was attached to the notch to measure the strain.

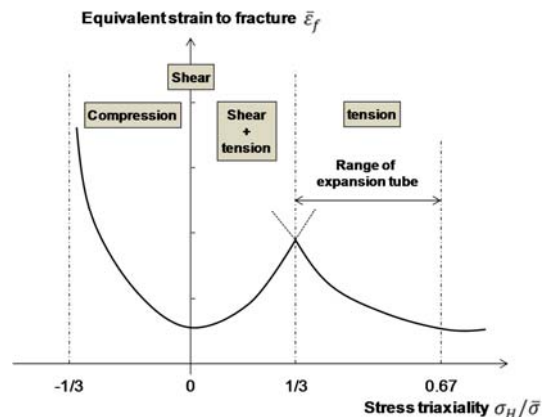


Fig. 1 Variation of equivalent strain to fracture with respect to stress triaxiality

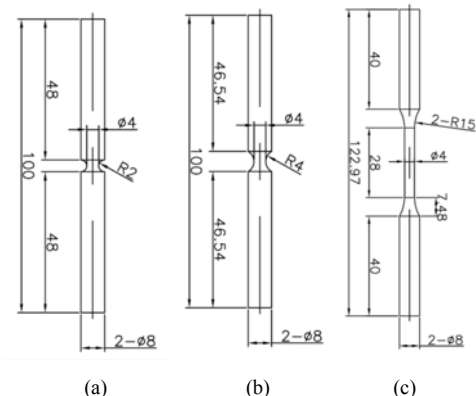


Fig. 2 Specimen configurations for tensile test: (a)  $R=2$ mm, (b)  $R=4$ mm and (c)  $R=\infty$  mm

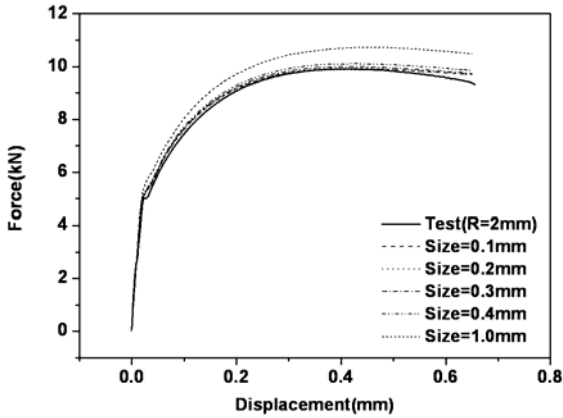


Fig. 3 Comparison of specimen test ( $R=2\text{mm}$ ) to finite element analysis with variation of mesh (0.1mm~1.0mm)

*B. Effect of mesh size*

Because the stress and rupture strain occurring on the element vary depending on the mesh size, the appropriate mesh size was determined by comparing the results of a  $R=2\text{mm}$  specimen test, which is the most sensitive to the mesh size, with those of a finite element analysis. Fig. 3 shows the results of the analysis with changing mesh size, and the size matches the test results up to 0.3mm, but beyond that, a force greater than the test results was generated. Therefore, the failure strain and stress triaxiality were calculated from a specimen model with mesh size of 0.3mm. The same sized mesh was used for the tube analysis as well.

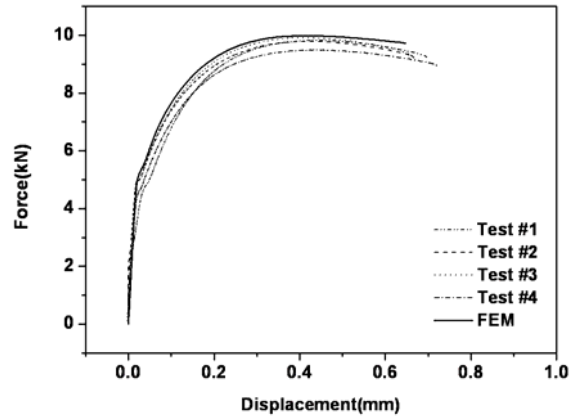
*C. FE analysis for calibration*

To calculate the failure strain and stress triaxiality, a finite element analysis was performed with the same conditions as the tensile test. Because rupture starts in the middle of the specimen, it has the highest stress triaxiality and strain [16, 17]. For the finite element analysis, 1/4 axisymmetric model was used, and the stress triaxiality and strain were calculated from the integral point of the middle element.

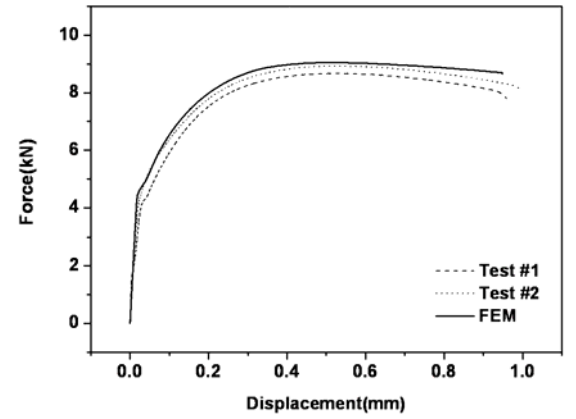
Fig. 4 shows the specimen test and analytical results, indicating that if the notch ( $R$ ) is small, the elongation becomes smaller but the force becomes greater. Table 1 shows the stress triaxiality and strain of the specimen's middle part at the point where necking and rupture begin.

Researches prior to Weirzbicki et al. represented the relation between stress triaxiality and failure strain at a high stress triaxial state as the exponential function shown in Equation [18]. Fig. 5 is a graph that approximates the stress triaxiality calculated from the specimen test as the exponential function, where  $K$  and  $n$  are 0.277 and -0.847, respectively.

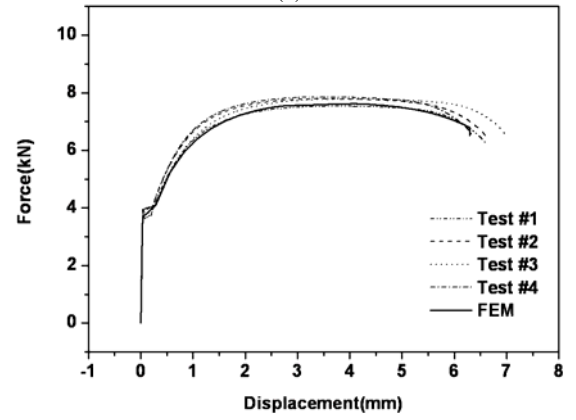
$$\bar{\epsilon}_f = K \left( \frac{\sigma_H}{\bar{\sigma}} \right)^n \tag{5}$$



(a)



(b)



(c)

Fig. 4 Result of specimen tests and finite element analysis with damage model: (a)  $R=2\text{mm}$ , (b)  $R=4\text{mm}$  and (c)  $R=\infty\text{mm}$

TABLE I  
FAILURE PARAMETERS WITH RESPECT TO NOTCH SHAPES ( $R$ )

R(mm)	NECKING		FAILURE	
	EQUIVALENT STRAIN	STRESS TRIAXIALITY	EQUIVALENT STRAIN	STRESS TRIAXIALITY
2	0.141	0.81	0.33	0.859
4	0.174	0.603	0.383	0.647
$\infty$	0.152	0.333	0.68	0.348

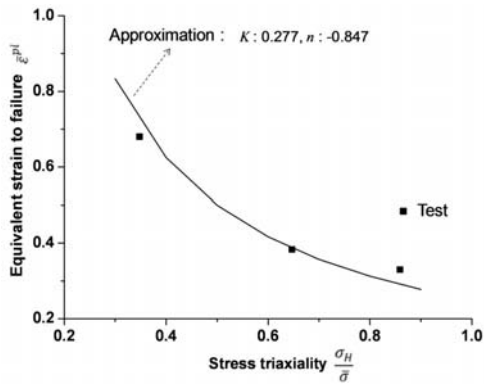


Fig. 5 Approximation of relationship between equivalent strain to failure and stress triaxiality

IV. PREDICTION OF RUPTURE

A. Determination of variable

Because rupture instability of the expansion tube is dominantly influenced by expansion ratio, the punch radius ( $R_p$ ), and the slope angle ( $\alpha$ ), which influence the expansion ratio among design variables of the punch, were chosen as variables, and a finite element analysis was performed by changing these two variables [5]. Fig. 6 is a schematic diagram for the expansion tube analysis, and Table 2 provides the primary dimensions and variable range of the punch and the tube.

B. Finite element model

Fig. 7 is a model for the finite element analysis of the expansion tube where the punch is assumed as a discrete rigid body, while the expansion tube consists of a four-node

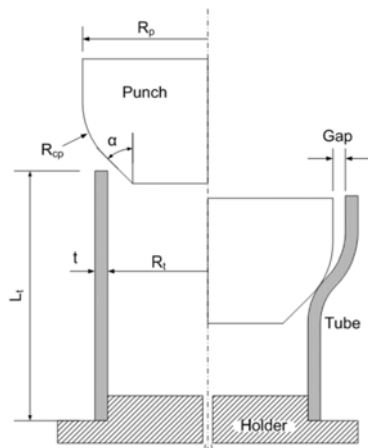


Fig. 6 Schematic diagram for finite element analysis

TABLE II  
PRIMARY DIMENSIONS

VARIABLE	$R_p$ (mm)	$R_i$ (mm)	$R_{cp}$ (mm)	$L_t$ (mm)	$t$ (mm)	$\alpha$ (deg)
Value	105,107.5, 110,115	93	20	350	11	15,30, 45,60

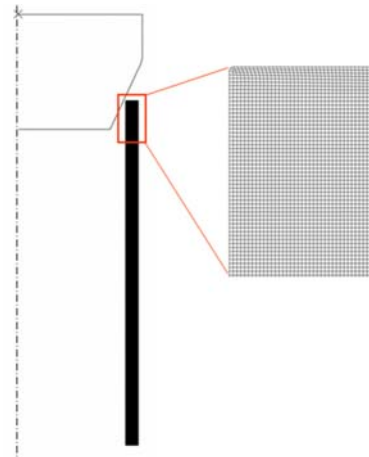


Fig. 7 Finite element model

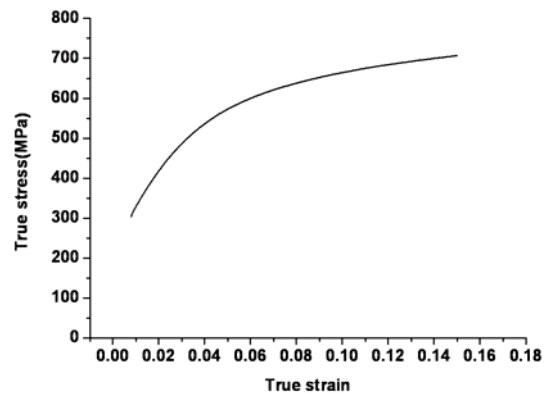


Fig. 8 True stress-true strain curve of SCM440

axisymmetric element with reduced integration point. Fig. 8 shows SCM440's true strain-stress linear diagram, where a finite element analysis was performed by assuming isotropic materials. Furthermore, the damage initiation criterion and shear failure conditions were applied to the finite element analysis in order to predict softening and failure of the tube.

While the amount of energy absorbed into the expansion tube is determined by material characteristics and friction conditions, rupture is influenced only by material characteristics irrespective of friction. Change in the friction conditions with respect to the punch shapes was not considered in the analyses. The shear friction factor of  $m=0.0421$ , which was calculated by comparison of the finite element analysis to quasi-static test ( $R_p=107.5\text{mm}$ ,  $\alpha=30^\circ$ ), was applied to all analyses [19].

V. RESULT OF FINITE ELEMENT ANALYSIS

Eq. (6) was derived from Eq. (5) to determine if there is a rupture among elements comprising the tube. If an element of the tube satisfies Eq. (6), that element is eliminated from the tube model. Outer surface on the tube experiences bending and unbending phenomenon during the expansion process. Because rupture takes place at the outer surface near the punch edge ( $R_{cp}$ ) where unbending occurs, the stress triaxiality and equivalent strain calculated from the outer elements of the tube

were substituted into Eq. (6), called as determinant of rupture, to determine the occurrence of a rupture.

$$D_f = \bar{\epsilon}^{pl} - K \left( \frac{\sigma_H}{\bar{\sigma}} \right)^n \begin{cases} \text{if, } D_f \geq 0 : \text{Failure} \\ \text{if, } D_f < 0 : \text{safe} \end{cases} \quad (6)$$

In Table 3,  $D_f$  calculated from the outer element of the tube depending on the punch radius and punch angle is rearranged, while Fig. 9(a) shows how  $D_f$  changes depending on the punch radius. Fig. 9(a) shows that at every punch angle except  $\alpha=30^\circ$ ,  $D_f$  increased when the punch radius increased. When  $\alpha=30^\circ$ ,  $D_f$  does not increase at  $R_p=107.5$  any further. When  $\alpha=45^\circ$  and  $50^\circ$ ,  $D_f$  was closer to 0 with  $R_p=110$ mm, and was larger than 0 with  $R_p=115$ mm, thereby satisfying the rupture condition ( $D_f \geq 0$ ). The cases of  $\alpha=45^\circ$  and  $50^\circ$  show nearly the same change up until  $R_p=110$ mm, but when it was higher, the case of  $50^\circ$  showed larger values than that of  $45^\circ$ . The graph presented in Fig. 9(b) illustrates the change of  $D_f$  depending on the punch angle, indicating that a specific punch angle exists except  $R_p=115$ mm where the  $D_f$  value no longer increases. Further, the specific punch angle increased along with the punch radius. Fig. 9(c) graphically displays the influence of the expansion ratio; if the punch angle is small, the rate of increase of  $D_f$  against the punch radius is low, and if the punch angle is large, the rate of increase of  $D_f$  against the punch radius is high. Fig. 10 shows the results of the finite element analysis with  $R_p=115$ mm,  $\alpha=45^\circ$ , indicating that a rupture occurs at the tube outer surface near  $R_{cp}$ .

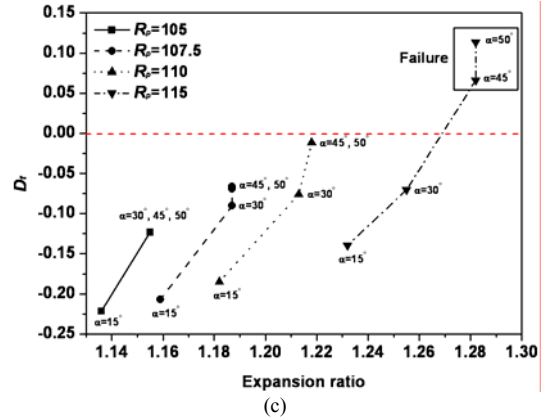


Fig. 9 Effect of key parameter of the punch and expansion ratio on the  $D_f$ : (a) punch radius, (b) punch angle and (c) expansion ratio

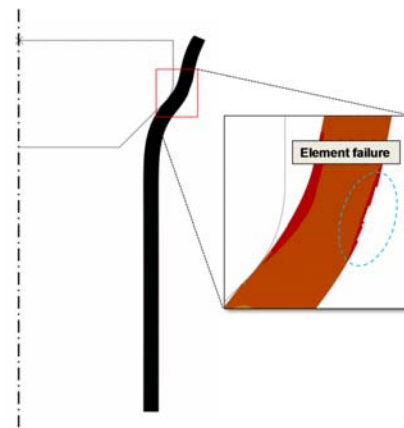
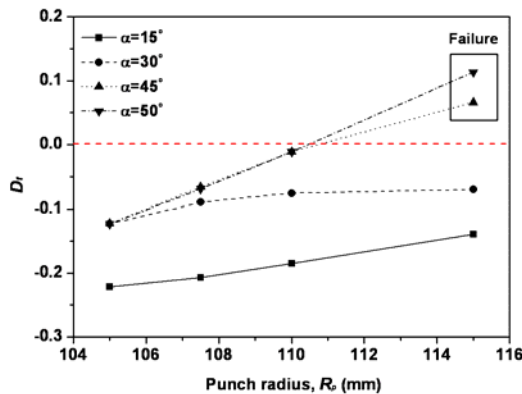
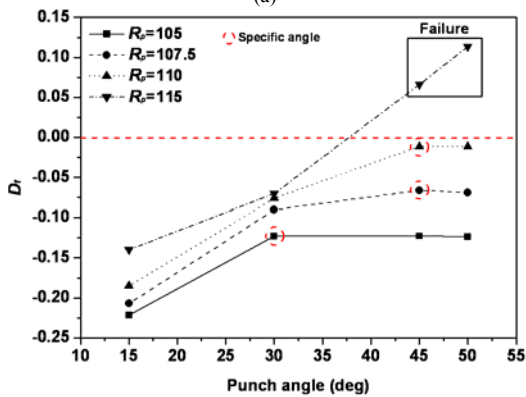


Fig. 10. Result of finite element analysis with  $R_p=115$ mm,  $\alpha=45^\circ$



(a)



(b)

TABLE III  
 $D_f$  AND EXPANSION RATIO ( $R_p/R_a$ )

$\alpha$ (deg)	$R_p=105$ mm		$R_p=107.5$ mm		$R_p=110$ mm		$R_p=115$ mm	
	$D_f$	$R_p/R_a$	$D_f$	$R_p/R_a$	$D_f$	$R_p/R_a$	$D_f$	$R_p/R_a$
15	-0.221	1.136	-0.207	1.159	-0.185	1.182	-0.14	1.232
30	-0.123	1.155	-0.09	1.187	-0.076	1.213	-0.07	1.255
45	-0.123	1.155	-0.066	1.187	-0.011	1.218	0.066	1.282
50	-0.123	1.155	-0.069	1.187	-0.011	1.218	0.114	1.282

## VI. RESULT

In order to study how the punch radius ( $R_p$ ) and punch angle ( $\alpha$ ), the main design factors of the punch, affect rupture of the tube in an analytical manner, finite element analyses were performed by applying a damage initiation criterion, a damage model for ductile material, and a shear failure model while changing the punch radius and the punch angle. In addition, tensile strength tests were performed on tensile specimens with three notch shapes to ensure precise prediction of the tube's rupture, and the failure strain based on the stress triaxiality was calculated and applied to the finite element analysis.

The analysis revealed that no rupture occurred at the tube even when  $R_p$  was as large as 115mm if the punch angle was lower than  $\alpha=30^\circ$ . However, if the punch angle becomes larger ( $\alpha=45^\circ, 50^\circ$ ), the tube ruptured when  $R_p$  was larger than

100mm. Therefore, the punch angle should not exceed  $30^\circ$  when it is made greater to increase the amount of energy absorption with a larger tube expansion ratio. For other punch outer diameters, i.e., except when  $R_p=115\text{mm}$ , there existed a specific punch angle whose  $D_f$  value did not increase even when the punch angle is increased. This specific punch angle increased along with an increase in the punch radius. While  $D_f$  is influenced by the expansion ratio, it did not grow in proportion. Meanwhile, the expansion ratio is influenced more by the punch radius than by the punch angle, whereas  $D_f$  is influenced more by the punch angle than by the punch radius. In other words,  $D_f$  is small when the punch angle is small, even when the punch radius is large. However, the amount of plastic deformation occurring at the tube is influenced by both the punch radius and the punch angle. However, the amount of plastic deformation near  $R_{cp}$  where a rupture occurs on the tube is influenced more by the punch angle than by the punch radius, and the tube's rupture is influenced more by change in the punch angle than by the punch radius.

## REFERENCES

- [1] M. Shakeri, S. Salehghaffari, R. Mirzaeifar, "Expansion of circular tubes by rigid tubes as impact energy absorbers: Experimental and theoretical investigation," *Int. J. Crashworthiness.*, vol. 12, 2007, pp. 493–501.
- [2] V. Lucanin, J. Tanaskovic, D. Milkovic, S. Golubovic, "Experimental Research of the Tube Absorbers of Kinetic Energy During Collision," *FEM Trans.*, vol. 35, pp. 201–204, 2007.
- [3] A. Karrech, A. Seibi, "Analytical model for the expansion of tubes under tension," *J. Mater. Process. Technol.*, vol. 210, 2010, pp. 356–362.
- [4] T. Daxner, F. G. Rammerstorfer, F. D. Fischer, "Instability phenomena during the conical expansion of circular cylindrical shells," *Comput. Method. Appl. Mech. Eng.*, vol. 194, 2005, pp. 2591–2603.
- [5] B. P. P. Almeida, M. L. Alves, P. A. R. Rosa, A. G. Brito, P. A. F. Martins, "Expansion and reduction of thin-walled tubes a die : Experimental and theoretical investigation," *Int. Journal. Mach. Tools. Manuf.*, vol. 46, 2006, pp. 1643-1652.
- [6] H. Hooputra, H. Gese, H. Dell, H. Werner, "A comprehensive Failure Model for Crashworthiness Simulation of Aluminium Extrusions," *Int. J. Crashworthiness.*, vol. 9, No. 5, 2004, pp. 449–464.
- [7] ABAQUS User's Manual, Verson 6.6. Hibbit Karlsson and Sorensen Inc.
- [8] J. H. Holloman, *Trans. AMIE.*, vol. 162, pp. 268, 1915.
- [9] A. L. Gurson, "Continuum Theory of Ductile Rupture by Void Nucleation and Growth: Part I - Yield Criteria and Flow Rules for Porous Ductile Media," *J. Eng. Mater. Technol.*, 1977, pp. 2–15.
- [10] S. Ghosh, M. Li, A. Khadke, "3D modeling of shear-slitting process for aluminum alloys," *J. Mater. Process. Tehcnol.* vol. 167, 2005, pp. 91–102.
- [11] V. Uthaisangasuk, U. Prael, S. Münstermann, W. Bleck, "Experimental and numerical failure criterion for formability prediction in sheet metal forming," *Comput. Mater. Sci*;doi:10.1016/j.commatsci.2007.07.036.
- [12] J. R. Rice, D. M. Tracey, "On the ductile enlargement of voids in triaxial stress fields," *J. Mech. Phys. Solids.*, vol. 17, 1969, pp. 201–217.
- [13] M. G. Cockcroft, D. J. Latham, "Ductility and workability of metals," *J. Inst. Metals.*, vol. 96, 1968, pp. 33–39.
- [14] Y. Bao, T. Wierzbicki, "On fracture locus in the equivalent strain and stress triaxiality space," *Int. J. Mech. Sci.*, vol. 46, 2004, pp. 81–98.
- [15] G. Mirone, "Role of stress triaxiality in elastoplastic characterization and ductile failure prediction," *Eng. Fract. Mech.*, vol. 74, 2007, pp. 1203–1221.
- [16] Y. Bao, T. Wierzbicki, "A comparative study on various ductile crack formation criteria," *J. Eng. Mater. Technol.*, vol. 126, Issue 3, 2004, pp. 314–325.
- [17] J. W. Hancock, A. C. Mackenzie, "On the mechanisms of ductile failure in high-strength steels subjected to multi-axial stress-states," *J. Mech. Sci.*, vol. 31, 1996, pp. 453–61.
- [18] T. Wierzbicki, O. Muragishi, "Calibration of ductile fracture from compression and tension tests," *Impact & Crashworthiness Laboratory; Report No. 21; MIT; 1999.*
- [19] W. M. Choi, T. S. Kwon, H.S. Jung, "Quasi-static Experimental Study on Energy Absorbing Characteristic of Expansion Tube," *FISITA2010 World Automotive Congress, F2010D041, Scientific Society for Mechanical Engineering, 2010.*